EPJ Web of Conferences **99**, 04001 (2015)
DOI: 10.1051/epjconf/20159904001

Ultra-high energy cosmic rays: 40 years retrospective of continuous observations at the Yakutsk array: Part 1. Cosmic ray spectrum in the energy range 10^{15}–10^{18} eV and its interpretation

Stanislav Knurenko[a], Igor Petrov[b], Zim Petrov, and Ivan Sleptsov

Yu. G. Shafer Institute of cosmophysical Research and Aeronomy, 31 Lenin ave, Yakutsk, Russia

Abstract. The experimental data on the cosmic ray energy spectrum obtained from the Small Cherenkov Array in Yakutsk on the measurement of Cherenkov radiation in showers with energy 10^{15}–10^{18} eV are discussed. The data were obtained by means of continuous array operation since 1994. The all particle spectrum in this energy region was found to have a complex shape and cannot be described by a simple exponential function with a single slope indicator, g. After the first kink at energy $3 \cdot 10^{15}$ eV (knee), the spectrum becomes steeper at $\Delta\ \gamma = 0.4$ up to energy $< 2 \cdot 10^{16}$ eV, then part of the spectrum becomes flat to $>8 \cdot 10^{16}$ eV, the slope of the spectrum is 2.92 ± 0.03 and then again changes slope by $\Delta\gamma = 0.32 \pm 0.05$ from about $\sim 2 \cdot 10^{17}$ eV. The second kink in the spectrum observed at the Yakutsk EAS array at $\sim 2 \cdot 10^{17}$ eV, or also called second knee, is a significant result for space astrophysics of ultra-high cosmic rays. In this paper we discuss possible scenarios for spectrum formation of cosmic rays by galactic sources to energies $< 10^{17}$ eV, mainly supernovae remnants (SNR) and Metagalactic origins in the energy range 10^{17}–10^{18} eV. Most likely, that measurement of the second knee is related with the transitional region, galactic to extragalactic origin of cosmic rays.

1. Introduction

The main objectives of cosmic ray (CR) research of ultra-high energies are to determine the anisotropy of the energy spectrum and chemical composition of the primary CR particles. These characteristics of CR have an important role in understanding the origin, acceleration and propagation of the primary particle of different energies. In the energy range 10^{12}–10^{14} eV such measurements are carried out with the use of satellites and the launch of balloons at heights $\sim$35 km. These experiments allow a direct measurement of the chemical composition of the particles, and their partial spectra. The only disadvantage of these experiments is the low luminosity of the arrays and the limited time of observations. At energies higher than 10^{14} eV, because of the low intensity, the only method to study characteristics of the CR is by measuring extensive air showers (EAS), i.e. indirectly, tracking of cascade processes in the atmosphere and the registration of charged particles, muons, ionization and emission of Cherenkov light of EAS at sea level. Because of the wide range of energies of the primary particles, the registration of EAS is conducted on small arrays, the area of which is s $< 1\,\text{km}^2$ up to 10^{18} eV energy, medium arrays with area s $< 20\,\text{km}^2$ energies up to 10^{19} eV, and in very large arrays such as Auger and Telescope Array.

2. Experiments at Yakutsk

The main Yakutsk EAS array consists of small arrays with equipment designed to perform both general and specific objectives, such as the measurement of muons by the Large Muon Detector, the measurement of the profile of the cascade curve system by Cherenkov detectors, measurement of radio emission, monitoring of the atmosphere during the registration period of air showers etc. This equipment is controlled by a system of computers connected in a local network [1].

In 1994, a Small Cherenkov array was installed in the central part of the Yakutsk array to detect moderate energy EAS [2]. One of the tasks that had to be settled was to study the spectrum of cosmic rays (CR) in the energy range 10^{15}–10^{17} eV [3], where, according to [4], the manifestation of the fine structure in the spectrum of CR due to the interaction of cosmic ray particles with the magnetic field of the Galaxy was expected.

2.1. Current status of Small Cherenkov array

The main difference of the Small Cherenkov array from other compact arrays is that the array uses a hybrid type of registration of multiple air shower components: electrons, muons and Cherenkov radiation. It allowed us to determine shower energies [5] using a quasi calorimetric method, to reconstruct air shower cascade development [6], to plot the spectrum and estimate the mass composition of CR [7].

Figure 1 shows the Small Cherenkov array. It consists of 27 integral and track Cherenkov detectors with different reception areas: type 1 has an area of 176 cm^2 photocathode, Type 2 – 530 cm^2 and 17 scintillation

[a] e-mail: knurenko@ikfia.sbras.ru
[b] e-mail: igor.petrov@ikfia.sbras.ru

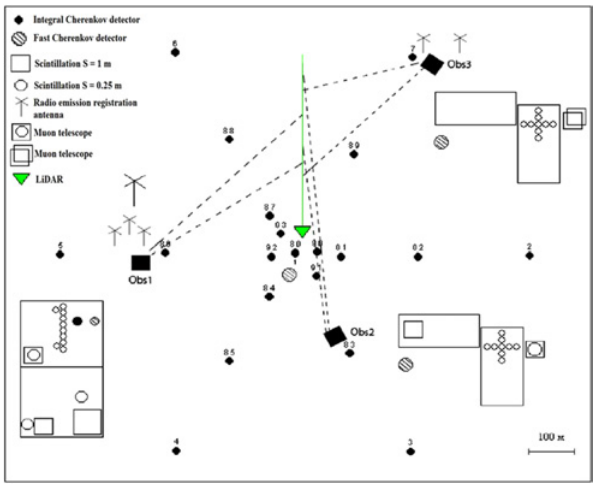

Figure 1. Arrangement of observation stations on the Small Cherenkov array.

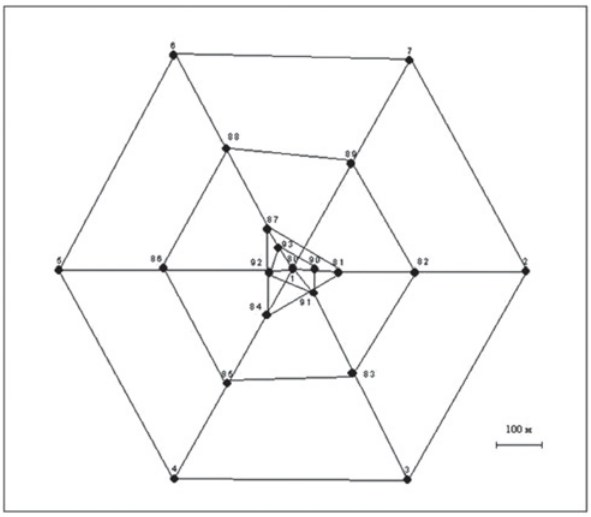

Figure 2. Configuration of trigger combinations used at the Small Cherenkov array.

detectors of different sizes, 2 m^2, 1 m^2, 0.5 m^2 and 0.25 m^2 each. The stations are arranged at 25, 50, 100, 250 & 500 m from each other. The array also consists of 3 muon telescopes with a threshold of 1 GeV. Stations at distances of 500 m from the center are not connected directly to a main registration point but their data are used in the processing of events registered at the same time by both units.

2.2. Event selection

Figure 2 shows the location of stations involved in the selection of air shower events with energies 10^{15}–10^{18} eV. EAS were selected by coincidence signals from stations that make up an equilateral triangle for 2.5 μs. To plot a spectrum of CR we used the following criteria to select air showers from the collected data: coefficient of atmospheric transparency was $P_\lambda \geq 0{,}65$; shower axis was located within the perimeter of the array with a radius $R \leq 500$ m; the zenith angle of arrival of the EAS $\theta \leq 50^\circ$. These criteria were determined first of all by aperture, threshold

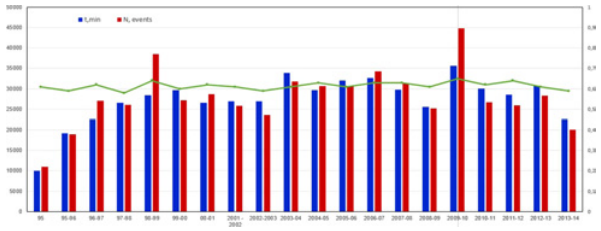

Figure 3. Small Cherenkov array. Statistics of showers with energy more than $2 \cdot 10^{15}$ eV. Blue bars–time of observation in minutes. Red bars–number of registered air shower events. Green line–average spectral transparency of the atmosphere for wavelength $\lambda = 430$ nm.

of Cherenkov detectors and state of the atmosphere during optical observation.

2.3. Observations

The small Cherenkov array has worked continuously for 20 years. The duty cycle of the array is from September to April, during moonless, clear nights. Figure 3 shows the work time of the array by years for the whole observation period and average spectral transparency of the atmosphere for wavelength 430 nm [8].

3. Simulation

The simulation algorithm includes not only brute force search of triangles, but also accounts for the threshold of detectors and their fluctuations in backlight conditions when measuring the flow of Cherenkov photons. In each case, the selection of air shower events analyzed coincidence criterion for 2.5 μs, signals from three stations constituting an equilateral triangle with a different base for the distance, i.e. C3. Exceptions were stations of the Small Cherenkov array that make up triangles with sides of 100, 50 and 25 m. This case also considered triggers of the other triangles or even quadruple coincidence. The purpose of these triggers was to improve the efficiency of event selection in the transition region from energies of 10^{15} eV to $5 \cdot 10^{15}$ eV. Since EAS events of different energies were selected by different trigger systems, the transition from one trigger that selects showers with less energy to the trigger that selects showers with more energy should give the effect. This is understandable, since at some point the trigger system changes as well as the effective area of air shower detection. Simulations showed that the magnitude of this effect is ~30%. In our case an account of the transition effect to plotting the spectrum decreased from 30% to 15% due to the correction of area of air shower detection.

3.1. Precision of obtained air shower characteristics

The precision of measurements of air shower characteristics was determined by simulation of Small Cherenkov array measurements, using Monte Carlo method. The results are shown in Table 1. The table shows that EAS characteristics used in the analysis are determined with a

Table 1. Precision of EAS characteristics measurements achieved at the Yakutsk array.

E_0,PeV	σ(R), m	δN_s	σ(Q(100)) phot/m^2	σ(Q(200)) phot/m^2	σ(Q(400)) phot/m^2	$\sigma(\rho_s(300))$ 1/m^2	$\sigma(\rho_s(600))$ 1/m^2	θ°
2	9.7	0.15	0.17					1.3
10	7.2	0.11	0.15					1.0
100	15.5	0.27	0.15	0.25				5.7
200	34.6	0.32	0.20	0.20	0.22	0.25		5.4
1000	26.7	0.35	–		0.20	0.17	0.19	3.3

Table 2. The energy transferred to the different components of the EAS.

n/n	lg $E_e i$	lg $E_e l$	lg E_μ	lg E_{hi}	lg(E_{mi}+E_ν)	lg E_0
1	15.687	14.506	14.840	14.465	14.721	15.823
2	15.830	14.612	14.951	14.608	14.832	15.961
3	16.064	14.876	15.175	14.842	15.056	16.195
4	16.345	15.199	15.410	15.123	15.291	16.471
5	16.540	15.362	15.506	15.318	15.387	16.650
6	16.669	15.473	15.644	15.447	15.526	16.783
7	16.797	15.726	15.783	15.575	15.664	16.916
8	16.874	15.851	15.899	15.652	15.780	17.002
9	17.014	16.001	16.015	15.792	15.896	17.139
10	17.116	16.122	16.081	15.894	15.962	17.238
11	17.208	16.269	16.173	15.986	16.054	17.334
12	17.297	16.435	16.306	16.075	16.187	17.436

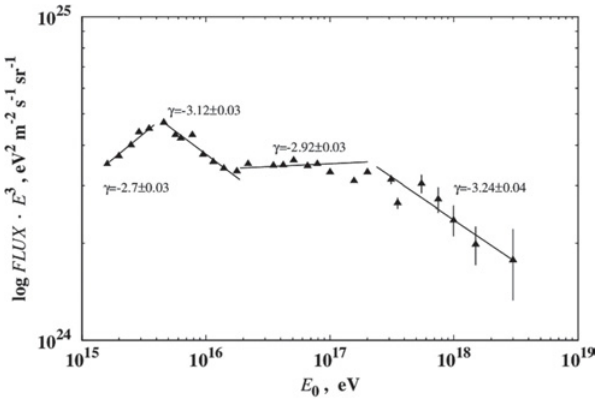

Figure 4. A spectrum of cosmic rays in the region 10^{16}–10^{18} eV by Yakutsk data. There is a second knee at energy $\sim 2 \cdot 10^{17}$ eV.

good precision and we used them for further determination of individual air shower energies.

Under real conditions, there is a significant contribution of the light loss by aerosol particles with different sizes. Some uncertainty also makes extreme subarctic climate in the region of the array, i.e. during winter above the array sits an abnormal atmosphere the properties of which change dramatically from autumn to winter and vice versa. Because of that, continuous observations of the atmosphere during periods of optical observations are conducted at the Yakutsk array [8,9] and data on the transparency of the atmosphere are taken into account in the determination of some characteristics of air showers.

3.2. Energy of the shower estimation. Energy balance method

Evaluation of the shower energy was determined using the method and the experimental data presented in [5,10]. Table 2 shows the results of the partial energies measured by the array for each of the components of EAS. Their sum is the evaluation of the total energy of the shower. According to the results of Table 2 the connection formula of the shower energy and density of Cherenkov light flux at distances of 100 m and 150 m–Q(100) & Q(150) was derived. Formulae 1 & 2 are valid for the energy range (2–500)·10^{15} eV and were used to plot the cosmic ray spectrum

$$E_0 = (5.75 \pm 1.39) \cdot 10^{16} \cdot (Q(100)/10^7)^{0.96\pm0.03} \quad (1)$$

$$E_0 = (9.12 \pm 2.28) \cdot 10^{16} \cdot (Q(150)/10^7)^{0.99\pm0.03}. \quad (2)$$

It is significant that the method is based on experimental data and does not depend on models of hadron interactions that describe the physics of EAS development in the atmosphere. Therefore, the method used for determining the shower energy at the Yakutsk array is more realistic, unlike other systems where energy is used to determine one or two versions of the models.

4. Air shower energy spectrum

From the data obtained at the Yakutsk Small Cherenkov array from 1994 to 2014 and selected using the criteria described above, we evaluated the frequency of EAS events registered in a given energy range, δE, and zenith angle, $\Delta\theta_i$, per unit of effective area of the Small Cherenkov array. Further, by introducing corrections to the transition effect in the corresponding energy intervals, we have specified spectra in the energy ranges $2{\cdot}10^{15}$–$2 \cdot 10^{16}$ eV and $8{\cdot}10^{17}$–$3 \cdot 10^{18}$ eV. The final energy spectrum is shown in Fig. 4. To switch from a classification parameter Q(150) to the energy E_0 we used the energy balance method described above.

As one can see from Fig. 4, the spectrum above 10^{15} eV has a complex shape and cannot be described by a single power law in the energy range from 10^{15} eV to 10^{18} eV. Even if we take into account the presence of systematic errors for plotting the spectrum (see Modelling section), its shape does not change much and marked irregularities in the spectrum at $\sim 3{\cdot}10^{15}$ eV and $\sim 2 \cdot 10^{17}$ eV are not going to disappear.

Let us approximate the spectrum by a simple power law function:

$$dN/dEdAd\Omega dt = I_0(E/1eV)^{-\gamma+1}. \quad (3)$$

We determined constant coefficients of equation 3 for four energy intervals. The first knee is characterized by

slopes $\gamma_1 = 2.70 \pm 0,03$ and $\gamma_2 = 3.12 \pm 0.03$, and the second knee by $\gamma_1 = 2.92 \pm 0.03$ and $\gamma_2 = 3.24 \pm 0.04$. In the second case, the difference of the slopes is $\Delta\gamma_{23} = (0.32) \pm 0.03 \pm 0.05$, which is less than that in the case of the first knee $\Delta\gamma_{12} = (0.42) \pm 0.03 \pm 0.05$. We can assume that the less distinguished kink in the spectrum may be due to the cosmic ray flux of a different nature, such as the influx of metagalactic components to our galaxy.

4.1. Comparison of the spectrum with other arrays results

Figure 5 shows the combined spectrum in the energy range 10^{15}–10^{18} eV, obtained at different arrays. There is good agreement with the shape of the spectrum obtained at the Yakutsk array and these data are consistent with the hypothesis of a second knee at $\sim 2{\cdot}10^{17}$ eV. The analysis showed:

a) the shape of the spectra in the energy range 10^{15}–10^{17} eV is the same and repeats of each other;

b) the intensities have spread between arrays in the range ~20%, it is more clearly visible at energies above $5{\cdot}10^{16}$ eV. This is partly due to the different methods for estimating the energy in each of the EAS arrays and to some extent different effective thresholds of the arrays themselves. Much greater variation in the intensity of the spectrum is observed above the energy $2{\cdot}10^{17}$ eV. On the one hand all the settings indicate a kink in the spectrum, but the degree of change in the slope of the spectrum is different. A much larger spread in the intensity of the spectrum is observed above the energy $2{\cdot}10^{17}$ eV. On the one hand all arrays indicate a kink in the spectrum, but the degree of change in the slope of the spectrum is different. For example, the data of Yakutsk and Tunka arrays are in better agreement with the data of large arrays Hires and TA, while data of KASCADE-Grande and Tibet III are in better agreement with Auger. It is possible that these aredue to the same reasons as listed above. However, it should be noted that for energies above 10^{17} eV air showers statistics at arrays such as Tibet III, Gamma are insufficient to clearly say with which of the large arrays they are in better agreement.

The Yakutsk Small Cherenkov array has the highest statistics of EAS in the energy range 10^{17}–$2 \cdot 10^{18}$ eV because it has run continuously for 20 years. As one can see from Fig. 5, its data are in good agreement with the data of HiRes array and TA.

Figure 6 shows the data of the Small Cherenkov array and new data of TALE Cherenkov and TALE Bridge. TA data are taken from ISVHECRI-2014. For energies above 10^{18} eV the results were obtained at TA during the last six years of observations. As one can see from Fig. 6, the data of the Yakutsk Small Cherenkov array are in very good agreement in the energy range 10^{16}–10^{18} eV with the new data of TALE Cherenkov and TALE Bridge, pointing to the second kink in the spectrum at $\sim 2 \cdot 10^{17}$ eV. At energies above 10^{18} eV there is also agreement of the spectra of

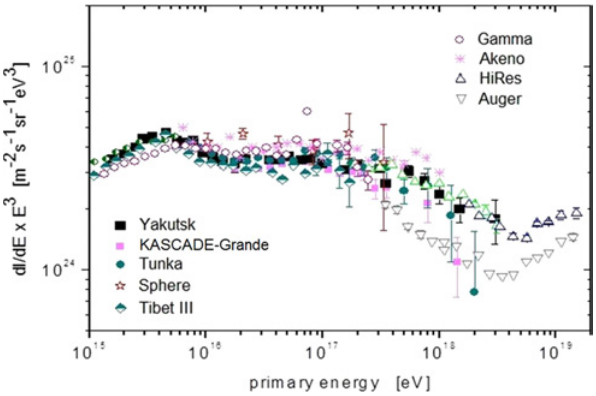

Figure 5. Cosmic ray spectrum for different arrays. Yakutsk data obtained from Small Cherenkov array.

both systems within experimental errors. As can be seen from Fig. 5, there is no agreement in spectra with the Auger experiment. The reason for such differences are likely related to the method of energy estimation made at the array. For example, the estimate of the energy of air showers obtained by the registration of energy loss by charged particles in the ionization of the atmosphere, in arrays TA, HiRes and the Yakutsk Small Cherenkov array, are within 5% with each other [5], which causes such a nice agreement of spectra.

4.2. Results discussion

The cosmic ray spectrum cut off due to iron nuclei leaving beyond the galaxy according to the Peters cycle [4] for a given magnetic field rigidity R_c should be observed at the cutoff energy $E_c = 26eR_c$, i.e. at $\sim 8{\cdot}10^{16}$ eV. According to the Yakutsk data the break exists at energies $\sim 2{\cdot}10^{17}$ eV. The actual change of slope is $\Delta\gamma = 0.32 \pm 0.07$ which is a bit less than in the case of the first break at energies $3{\cdot}10^{15}$ eV. For example, a little difference in slope $\Delta\gamma_{23}$ can be explained by cosmic ray injection from metagalactic sources [11], and thus some compensation of a dramatic change of slope at the break point in the energy range $5{\cdot}10^{16}$–$3{\cdot}10^{18}$ eV by protons and lighter nuclei from metagalaxy. In this case we can assume that the boundary between galactic and metagalactic CR, with a great possibility, lies in the energy region $2{\cdot}10^{17}$–$3{\cdot}10^{18}$ eV. Another explanation for the second break of the spectrum would be the contribution of one or even multiple sources of cosmic rays such as SNR with maximum luminosity.

4.3. Nearby sources which provide transition region from galactic to extragalactic CR

Paper [12] hypothesized about the transition region from galactic to extragalactic cosmic rays in the energy range 10^{17}–10^{18} eV. The latest spectrum data of Small Cherenkov array confirms that [13].

Following the idea that SNR are candidates for sources of cosmic rays, calculations were made [14] for the three propagation models of galactic and metagalactic components in the universe (see Fig. 7). The purpose of these calculations was the interpretation of the

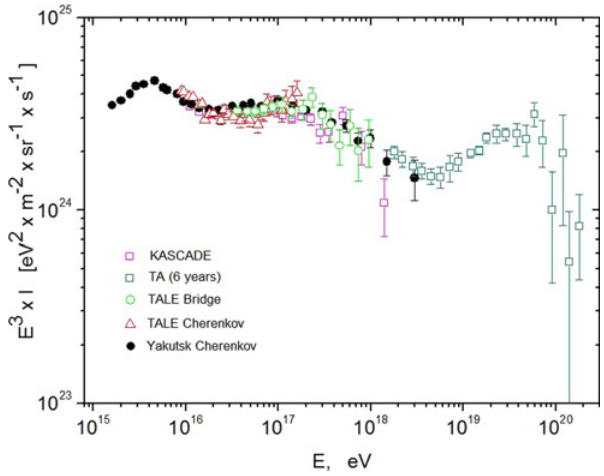

Figure 6. Experimental data of differemt experiments.

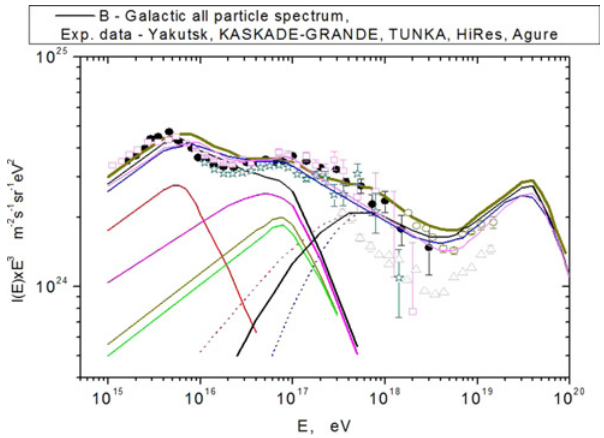

Figure 7. All particle spectrum measured by different experiments: Yakutsk, KASCADE Grande, Tunka and HiRes, Auger. Calculations [14,15]. Galactic cosmic rays are presented separately: dark green line (total), red line (H+He), blue line (Z>6), green line (Z>14), orange line (Z>20). Dot lines denote 3 fits of extragalactic protons, covered predictions [14]. Thick lines of the same colours represent galactic + extragalactic particles.

experimental spectrum in the energy range 10^{15}–10^{20} eV, obtained according to the compact and large EAS arrays. In particular it attempted to explain the formation of the second knee as the birth and propagation processes of cosmic rays in the galaxy and beyond. Calculations [14] have shown that the behavior of protons in the energy range 10^{16}–10^{17} eV depends on the average strength of the magnetic field $B_0 = 0.3$–3 nG, the coherence length lc 30–300 kpc, the source density $n = 10^{-5}$–10^{-6} Mpc^{-3} and other factors. For protons born outside the galaxy, as shown by calculations [11,14], an open proton spectrum will be in the range of energies 10^{17}–10^{18} eV. Data about the CR spectrum obtained recently at the compact array can serve as proof of this.

Figure 7 shows the partial spectra for individual nuclei and total spectra of all particles separately for the galactic component (obtained in [15], using the above described assumptions about the magnetic fields, the source model and varying the chemical composition of the particles to the galactic component). It is believed that cosmic rays are produced and accelerated in SNRs to energies E_{max} by the law $N\ (> E_{max}) \sim E_{max}^{-0.17}$ [14] and the upper limit of the acceleration of galactic cosmic rays $E = 26 \cdot (4 \pm 1)$ PeV. The spectrum in the source had the inclination $\gamma \sim -2.2$ up to E_{max} and becomes steeper on the value $d\gamma \sim -1.5$ higher energy E_{max} that imitated a break in the spectrum. The chemical composition of cosmic rays at the source has been selected as "normal" (∼36% of H, ∼24% of He, ∼10% of CNO, ∼9% of Fe), at an energy of 1 TeV. To describe the spectrum of heavy nuclei at energies $\sim 10^{18}$ eV cosmic rays in SN Ia remnants corrected by iron nuclei, increase their share to 15%. Ultimately, the chemical composition of galactic cosmic rays at 1 TeV becomes different from "normal" composition (17% of H, 46% of He, 8% of CNO, 16% of Fe). Thus calculations of the spectra obtained in [15] practically coincide with the experimental data, indicating the existence of a second knee in the energy range 10^{17}–10^{18} eV, i.e. at $\sim 2 \cdot 10^{17}$ eV. Thus, a second knee, as predicted in obtained in [14] and shown by calculations [15], formed by a sharp steepening of the spectrum of galactic iron nuclei in the energy range $(2–8) \cdot 10^{16}$ eV at $4 \cdot 26$ PeV and growth of contribution of metagalactic protons from $2 \cdot 10^{16}$ eV, which leads to the formation of the second knee.

5. Conclusion

Through 20 years of continuous observations and statistics of EAS events above 10^{17} eV the Yakutsk experiment has advanced the study of the CR spectrum in the energy range 10^{16}–10^{18} eV.

CR spectra obtained at the Small Cherenkov array indicate the existence of a second knee at $\sim 2 \cdot 10^{17}$ eV. There is reason to believe that the physics of the observed second break (kink) is associated with astrophysical processes occurring both within our own Milky Way galaxy as well as beyond our galaxy.

Relatively smaller difference in $\Delta\gamma$ between the first and second break points can be explained by the transition border from galactic to metagalactic cosmic rays. Most likely sources of cosmic rays in the energy range 10^{15}–10^{18} eV could be supernova remnants.

The research was supported by "Scientific and Educational Foundation for Young Scientists of Republic of Sakha (Yakutia)" (N 201302010098), Presidium SB RAS (integration project "Modernization of Yakutsk array"), RFBR (grant 13-02-12036 ofi_m).

References

[1] V.P. Artamonov *et al.* Bulletin of the Russian academy of Sciensec **58**, 92–97 (1994)
[2] S.P. Knurenko *et al.* Science and Education **4**, 46–50 (1998)
[3] S.P. Knurenko *et al.* Proc. 27 ICRC **1**, 145–147 (2001)
[4] B. Peters. Nuovo Cimento XXII, 800–819 (1961)
[5] S.P. Knurenko, A.A. Ivanov, I. Ye. Sleptsov, A.V. Sabourov. JETP Letters **83**, 563–567 (2006)
[6] S.P. Knurenko, V.A. Kolosov, I.T. Petrov *et. al.* Proc. 27 ICRC **1**, 157–160 (2001)

[7] S.P. Knurenko, A.A. Ivanov, A.V. Sabourov. JETP Letters **86**, 709–712 (2007)
[8] S.P. Knurenko, S.V. Nikolashkin, A.V. Saburov, I.Ye. Sleptsov/ Proc of SPIE **6522** (2006)
[9] S. Knurenko & A. Sabourov. J. Phys.: Conf. Ser. **409** (2013). doi: 10.1088/1742-6596/409/1/012083
[10] S.P. Knurenko *et al.* Proc 33 ICRC, report HE(2013)
[11] V.S. Berezinsky *et al.* Astrop. Phys. (2004) arXiv:astro-ph/0403477
[12] E.G. Berezhko, S.P. Knurenko, L.T. Ksenofontov. Astrop. Phys. **36** 31–36 (2012)
[13] S.P. Knurenko *et al.* Proc 33 ICRC (2013) arXiv:1310.1978v1 [astro-ph.HE]
[14] K. Kotera and M. Lemoine. (2008) arXiv: 0706.1891v2 [astro-Ph]
[15] L.G. Sveshnikova, E.E. Korosteleva, L.A. Kuzmichev *et al.* Proc. 33 ICRC (2013)